Supplemental Information
" Phase segregation of Sulfonate Groups in Nafion Interface Lamellae, Quantified via Neutron Reflectometry Fitting Techniques for Multi-layered Structures"

Steven C. DeCaluwe[a,b], Paul A. Kienzle[b], Pavan Bhargava[b,c], Andrew M. Baker[b,d], Joseph A. Dura[b]

a. Department of Mechanical Engineering, Colorado School of Mines, Golden, CO 80401
b. NIST-Center for Neutron Research, Gaithersburg, MD, 20899
c. Department of Electrical Engineering, University of Maryland, College Park, MD, 20742
d. Department of Mechanical Engineering, University of Delaware, Newark, DE, 19711

Controlled RH Sample Environment

As mentioned in the manuscript, care was taken to maintain stable and consistent control of the thermal environment and humidity, using the custom-built sample environment shown schematically in Figure S1, in order to minimize variations in Nafion water uptake at high RH values. Dry Ar carrier gas was first passed through a dew point generator, DPG, (*Li-Cor, Inc.*)[1], which itself was housed inside a controlled-temperature enclosure. The flow-rate was controlled at (240 ± 70) cm^3/minute via a needle valve, based upon observations of a flowmeter positioned at the entrance of this DPG enclosure. From there, the humidified gas travelled through a controlled-temperature heated line to the sample environment, which is a temperature-controlled Al cylinder (Al transmits neutrons with very little attenuation)

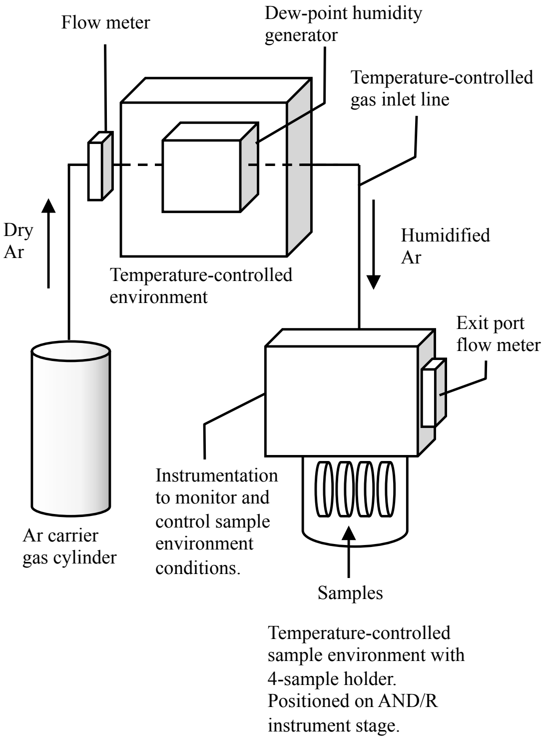

Figure S1. Schematic of measurement setup for RH control.

positioned on the goniometer stage of the instrument. Resistive heaters were attached above and below the neutron window to minimize temperature gradients. Control instrumentation, including gas inlet and outlet, an in-line RH sensor in the gas outlet, a flow meter at the gas outlet for leak detection, as well as electrical feedthroughs for temperature measurement and control, is housed on a flange which lies above and seals the sample cylinder. This flange is surrounded by a temperature-controlled enclosure. All temperatures in the carrier gas path other than the sample temperature are actively controlled at a constant temperature via K-type thermocouples and resistance heaters to maintain temperatures well above the dew point.

Up to four samples can be held in the sample environment at one time, and are kept in good thermal contact with the sample heater by polished aluminum clamps mounted to a Cu block at the top flange of the sample can. The sample temperature is controlled by simultaneous heating, via a resistive cartridge heater attached to the Cu block at the sample mount and actively controlled using a Pt thermometer, and cooling, via coolant loop filled with an ethylene glycol/water mixture maintained at a constant temperature by a water chiller.[2] The sample temperature is monitored via a calibrated Cernox sensor (*Lakeshore Cryotronics, Inc.*) attached to one of the samples by a clamp with a polished mating face placed outside of the neutron beam path. The RH at the sample was determined by two methods, which agreed to within the experimental uncertainty: (*i*) comparison of the specified dew point and the sample temperature, and (*ii*) via RH probe (*Rotronics*) positioned within the sample can, which is properly adjusted for the difference in temperatures between the sample and the RH probe. The dew point generator maintains the set point with a resolution of ± 0.01 °C with an uncertainty of ± 0.2 °C, and the combined heating and cooling keeps the sample temperature stable to within ± 0.02 °C of the set point. The Cernox sensor is accurate to within ± 0.04 °C; additional uncertainty due to the electronic uncertainty of the Lakeshore 340 controller brings the overall sample temperature uncertainty to ± 0.2 °C. The overall RH uncertainty is therefore 1.5 % for this experiment.

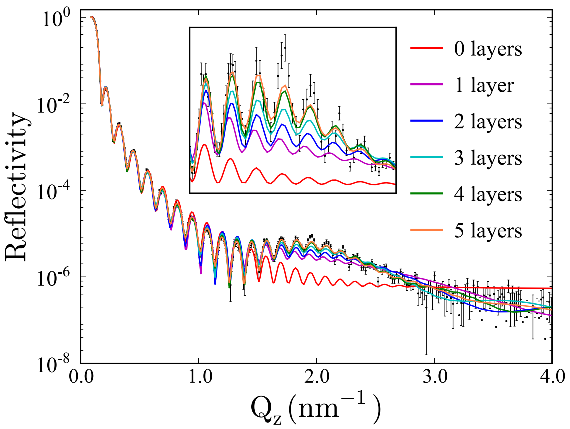

Figure S2. Fits to NR data taken on sample t42, 92 % RH, with varying numbers of lamellae. As the number of lamellae increases, the fit in the region of the high-Q lamellar peak centered at $Q_z \approx 2.0$ nm^{-1} improves noticeably. The inset focuses on this high-Q peak.

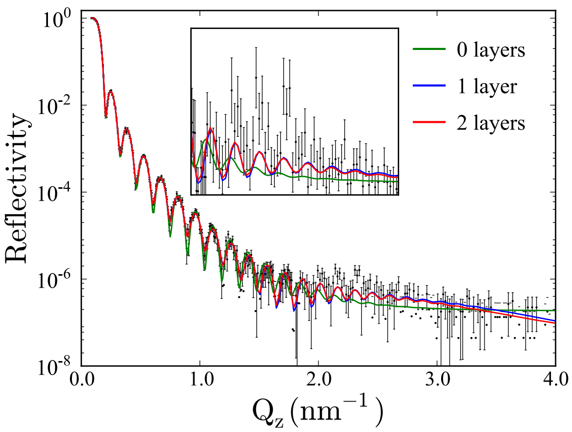

Figure S3. Fits to NR data taken on sample t42, 0 % RH, with varying numbers of lamellae. As the number of lamellae increases, the fit in the region of the high-Q peak associated with the remnant lamellar structure, centered at $Q_z \approx 2.2$ nm^{-1}, improves noticeably. The inset focuses on this high-Q peak.

Sub-optimal Fits to t42 Data for Models With Too Few Lamellae

As described in the manuscript, NR data sets taken on sample t42 in 92 % and 0 % RH environments were best fit by models with 6 and 3 lamellae, respectively, at the Nafion-substrate interface. Models with greater numbers of lamellae fit the data with roughly equal χ^2 to these models or else the improvement in the fit was not enough to justify the extra model complexity. For models with fewer lamellae than the best fits, the goodness-of-fit χ^2 statistics increased rapidly, characterized by a poor fit to the data in the region of the high-Q peak that is attributed to the lamellar structure. In generally, fits with too few lamellae could not reproduce the high amplitude of this peak. This is shown in Figure S2 for models with $n < 6$ lamellae fit to the 92 % RH data, and in Figure S3 for models with $n < 3$ lamellae fit to the 0 % RH data.

The Equivalent Nafion Thickness t_{Naf} and the Importance of Preserving Inter-parameter Correlations

The uncertainty of derived values, determined from multiple fitting parameters, can in theory be calculated by propagating the error estimate from each individual parameter. However, this would ignore the significant correlations between the parameters. Using Markov-Chain Monte Carlo approaches, Refl1d draws a random sample of parameter sets from the post-fit population of models,

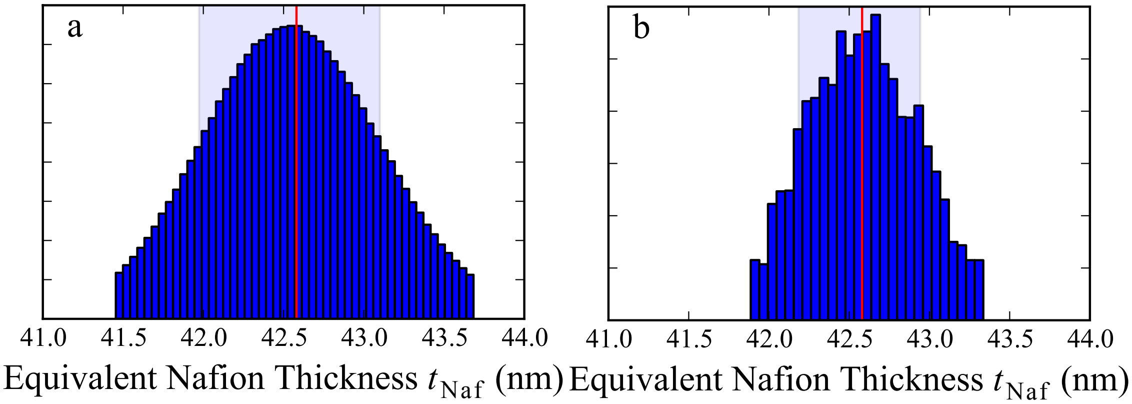

Figure S4. Total equivalent Nafion thickness (t_{Naf}) for sample t42 at 0 % RH. (a) Assuming all layers are independent - the histogram of t_{Naf} for each layer is generated separately and combined to obtain the total t_{Naf}. (b) Preserving inter-layer parameter correlations - t_{Naf} is determined for each parameter set before the histogram is generated. Shaded blue regions show 68 % confidence intervals. The red vertical lines show the value from the best fit.

and explicitly incorporates inter-parameter correlations by determining the derived value within each parameter set and then analyzing the disruption of these derived values to obtain the error estimate. The narrow confidence intervals for t_{Naf} presented in the main body of the manuscript demonstrate the utility of preserving parameter correlations in the Refl1d program. This is illustrated by the t_{Naf} histograms for the 6-lamellae fit to the 0% RH data, shown in Figure S4. Figure S4a demonstrates how propagating uncertainty values for the t_{Naf} calculation as though all layer parameters are independent (a sum of random distributions of $t_i V_{Naf,i}$) neglects the significant inter- and intra-layer correlations between parameters. This significantly overestimates the t_{Naf} uncertainty in Figure S4a [41.97 to 43.10] nm, compared to the [42.16 – 42.91] nm obtained when parameter correlations are properly preserved (a random distribution of sums of $t_i V_{Naf,i}$), as illustrated in Figure S4b.

Lamellar Layer Properties Variations With Increasing Distance From the SiO$_2$ Substrate

Figure S5 shows the fitted lamellae composition (V_{Water}) and thickness values for the damped oscillator model for layers 1 through 8, where layer 1 is adjacent to the SiO$_2$ substrate. Composition results in Figure S5a illustrate the oscillation between water-rich and water-poor layers, with increasing phase intermixing within layers further from the SiO$_2$ substrate increase. For layers 7 and greater, the layer composition is indistinguishable from that of the bulk-like outer layer (shown as the grey shaded area), as demonstrated by the overlap between the 68 % confidence intervals for layer and bulk V_{water} values. Accompanying this intermixing is an increase in layer thickness, as in Figure S5b, from 1.45 [1.37 – 1.54] nm adjacent to the SiO_2 to 1.94 [1.76 – 2.09] nm for layer 6.

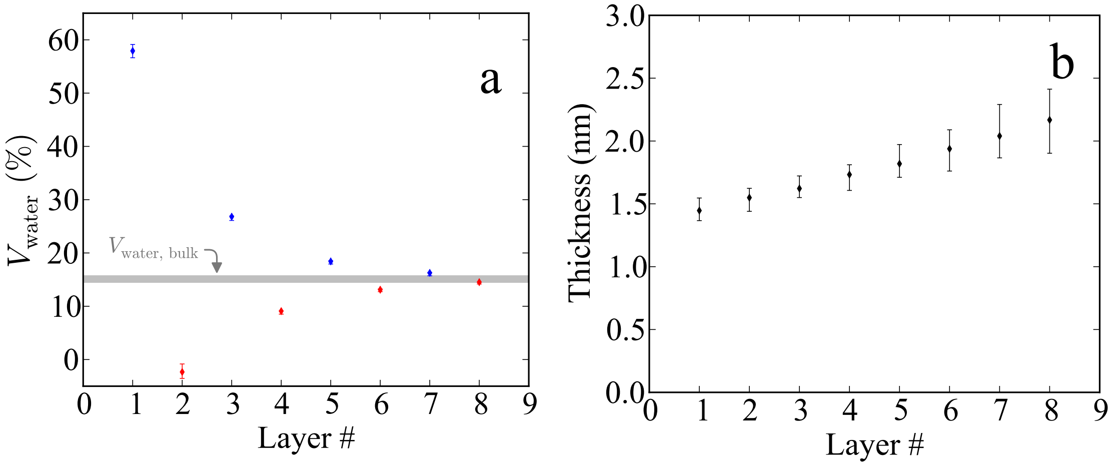

Figure S5. Sample t42 layer (a) compositions (V_{water}) and (b) thicknesses for the damped oscillator fit to 92% RH data. In Figure S4(a), blue and red data points represent water-rich and water-poor layers, respectively, and the grey shaded region shows the 68% confidence interval for the bulk-like outer layer. There is increasing intermixing of water-rich and -poor regions away from the SiO_2 substrate, with a composition that is statistically indistinguishable from the outer layer after 6 layers. In Figure S4(b), this intermixing is accompanied by increasing layer thickness away from the SiO_2 substrate. Error bars represent 68% confidence intervals.

Fits to t5 Data Without Isotope Contrast Variation

For sample t5, NR data was initially taken in 92 % RH with the carrier gas humidified by H_2O. Initial fits to this data resulted in numerous models with disparate SLD profiles that all gave suitable fits to the data (as characterized by low χ^2 values), as demonstrated in Figure S6. Figure S6a shows a collection of representative SLD profiles (offset on the y-axis for ease of visualization) that all gave suitable fits to the data. As can be seen, these profiles appear to be related by combinations of symmetry operations on sections and re-arrangements of these sections. Figure S6b shows the simulated NR data from these profiles, overlaid on the measured NR data, demonstrating that the piecewise-symmetry related models gave very similar fits to the data. Because NR data taken in H_2O vapor was incapable of distinguishing between these models, sample t5 was re-measured in 92 % RH

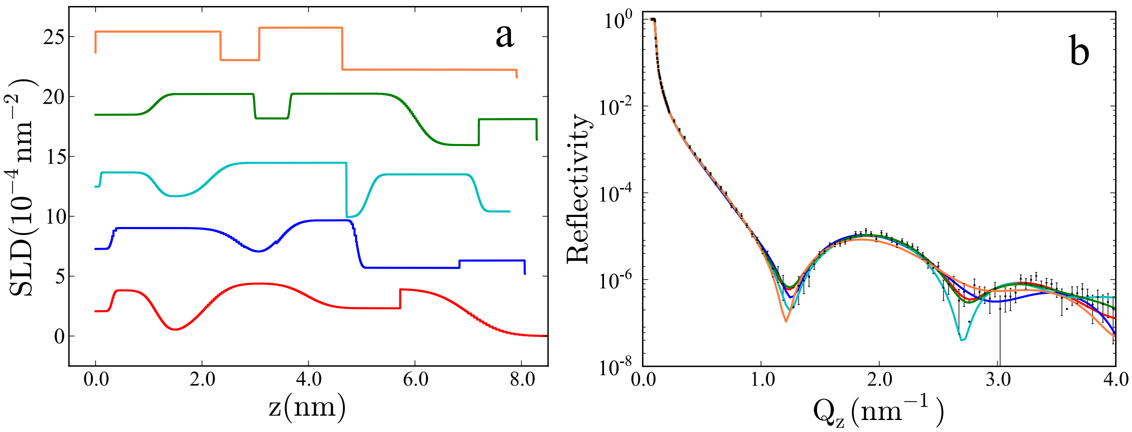

Figure S6. Multiple fits to NR data on sample t5 exposed to 92 % RH humidified by H_2O vapor. (a) Various and disparate SLD profiles (offset on the y-axis for ease of visualization) that all produced suitable fits to the NR data; (b) simulated NR data from the SLD profiles overlaid on the measured NR data, demonstrating the inability of the NR data to differentiate between the various models.

where D_2O was the humidifying isotope. As described in the manuscript, subsequent simultaneous fitting to the two data sets was capable of distinguishing between these models, and identified a single model that gave a suitable fit to the data and was also consistent with the lamellar SLD profile as identified previously[3] and in fits to sample t42. assumptions

The Composition Profile for Sample t5 with Each Layer Determined Independently from the SLD Profiles

As mentioned in the main body of the manuscript, once it is determined that the non-water composition in the t5 lamellae is not equal to that of Nafion 1100, calculating the lamellae compositions for sample t5 directly from the SLD values becomes mathematically under-determined. In order to close the system of equations with a limited number of the most reasonable suppositions, the following simplifying assumptions are made for sample t5: (*i*) given the wide range of possible compositions for lamella 1 suggested by the SLD confidence intervals in Figure 6a, the center of the 68 % confidence interval for the non-water SLD is used to calculate the composition of this lamella. Beyond this lamella, the non-water SLD profile from Figure 6a is used for all analysis; (*ii*) for the two lamellae adjacent to the SiO_2, where the non-water SLD is greater than that of Nafion 1100, it is assumed that there are no un-filled pores, since porosity would further decrease the non-water SLD below the value for Nafion 1100 rather than raise it to the determined values; (*iii*) for these same two lamellae, because the non-water SLD is between the values for FC groups and SO_3H (to within the experimental uncertainty) they are modeled as a mixture of these two components; (*iv*) in the two lamellae adjacent to the air interface, the non-water SLD is less than that of Nafion 1100; since this can be most easily explained by the presence of unfilled pores, we make that assumption, here; and (*v*) the remaining material (other than water and unfilled pores) in the two lamellae adjacent to the air interface will be considered to be bulk dry 1100 EW Nafion. The SLDs of the FC and SO_3H groups in assumption *iii* are derived from the SLD of Nafion 1100, approximating the density of the FC groups with that of PTFE, 2.2 g/cm^3. The resulting composition depth profile is shown in Figure 6b as a stacked area plot, with volume fractions summing to 1.0 at each *z*.

While these assumptions represent the minimum number required to close the system of equations, they do not result in a physically realistic composition profile. The resulting profile, as shown in Figure S7 violates the known stoichiometry of the 1100 EW Nafion – there are 1631 g of polymer per mole of SO_3H in the resulting composition profile. More specifically, layers 1 and 2 violate the Nafion 1100 stoichiometry by having too high a ratio of FC groups to SO_3H groups. Although this discrepancy can be corrected by adding SO3H groups to lamellae 3 and 4, as mentioned in the main text this is still not physically realistic, given the known length scales of the Nafion side-chains. Therefore the additional assumption, that the missing sulfonate groups are located as a partial monolayer at the substrate interface and in lamella 3 is required, leading to the physical model illustrated in Figures 6b and 7.

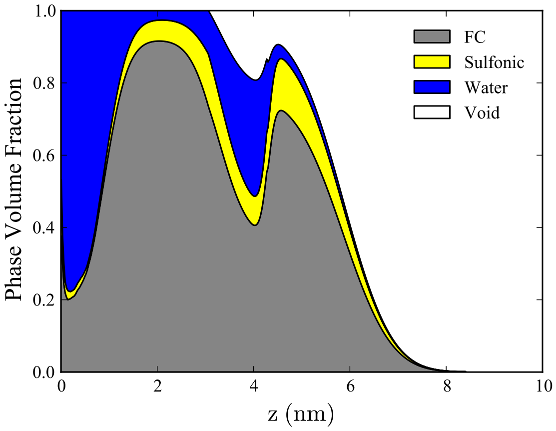

Figure S7. Composition depth profile for sample t5 under 92 % RH, employing the minimum number of reasonable assumptions. This model does not preserve the known stoichiometric ratio of SO_3H:FC groups for Nafion 1100.

References

(1) Bryngelsson, H., Stjerndahl, M., Gustafsson, T. & Edstrom, K. How dynamic is the SEI? *Journal of Power Sources* **174**, 970-975 (2007).

(2) Dura, J. A., Pierce, D. J., Majkrzak, C. F., Maliszewskyj, N. C., McGillivray, D. J., Losche, M., O'Donovan, K. V., Mihailescu, M., Perez-Salas, U., Worcester, D. L. & White, S. H. AND/R: Advanced neutron diffractometer/reflectometer for investigation of thin films and multilayers for the life sciences. *Rev. Sci. Instr.* **77** (2006).

(3) Dura, J. A., Murthi, V. S., Hartman, M., Satija, S. K. & Majkrzak, C. F. Multilamellar Interface Structures in Nafion. *Macromolecules* **42**, 4769-4774 (2009).